PAPER

Check for updates

NIR-light-triggered delivery of doxorubicin-loaded PLGA nanoparticles for synergistic cancer therapy on DMBA/TPA induced tumor-bearing mice†

Tunazzina Zaman Khan, ‡[a] Shekh Md Newaj, ‡[a] Ashikur Rahman, [a] Rahnuma Tabassum,[a] Khandaker Nujhat Tasnim, [a] Hasan Mahmud Reza,[a] Md. Selim Reza, [b] Seonki Hong [c] and Shazid Md. Sharker [a]

In this study, we developed NIR-light responsive poly(lactic-*co*-glycolic acid) (PLGA) nanoparticles (NPs) by incorporating the ICG dye for the local delivery of small-molecule drugs and therapeutics. Since NIR light can penetrate the skin up to a depth of 2 mm, it allows externally controlled photothermal-induced drug release. The synthesized NPs had a size of approximately 100 nm upon conjugation with a model anticancer drug, doxorubicin (Dox), which demonstrated *in vivo* NIR-derived heat generation exceeding 45 °C within 5 minutes. The *in vivo* efficacy of these NPs was evaluated by administering them *via* the tail vein route in DMBA/TPA-treated mice, resulting in a significant decrease in tumor size (from 15 to 1 mm^3). Histological results obtained from sacrificed tumor tissue also clearly supported the therapeutic activity of the developed NPs. This study indicates that NIR-guided PLGA-based NPs allow the localized delivery of therapeutics in a spatially controlled manner, potentially improving overall patient care.

1. Introduction

Localized delivery of anticancer drugs is crucial for both improving their therapeutic efficiency and minimizing undesirable side effects. Traditionally, chemotherapeutic drugs administered parenterally are distributed throughout the body *via* the systemic bloodstream, which causes cytotoxic anticancer effects not only in the tumor area but also in healthy tissues.[1,2] In this regard, strategies for the localized blood flow elevation in the intended tumor area, achieved through localized heat stimuli, have emerged to facilitate desired drug accumulation.[3] In cancer treatment, hyperthermia and photothermal therapy (PTT) are established clinical techniques in which heating the tumor area up to around 42 °C has been demonstrated to increase tumor cell death.[4] These elevated temperatures can also be utilized to enhance the local accumulation of chemotherapeutic drugs, synergistically improving overall treatment efficacy.[5]

Nanoparticles (NPs) have emerged in synergistic cancer therapies, serving as both NIR-derived heat generators and novel carriers for diverse therapeutic agents.[6] Several NP-based formulations have received FDA (US Food and Drug Administration) approval to date, such as biodegradable poly(lactic-*co*-glycolic acid) (PLGA) NPs, confirming their safety.[7] The primary advantages of NP-based drug carriers lie in their nanoscale size, which offers a substantial surface area for drug loading, and their ability to achieve passive tumor targeting through the enhanced permeability and retention (EPR) effect. Furthermore, NPs can be formulated with various functional motifs to respond to stimuli, including pH, temperature, light irradiation, and other external triggers, enabling spatiotemporal activation of NPs *in vivo* on-demand.[8] Inorganic NPs, such as superparamagnetic iron oxide nanoparticles (SPIONs) or gold nanorods, exhibit intrinsically high photothermal conversion efficiency, making them suitable for PTT.[9,10] However, addressing their cytotoxicity, in particular as the size decreases, remains a challenge. On the other hand, organic and/or polymeric NPs offer advantages in terms of dispersibility, degradability, and adaptability to various existing bioconjugate chemistries, which provide valuable strategies for fine-tuning the responsiveness of NPs to external stimuli.[11]

In this work, our objective was to design a nano-platform for NIR-induced localized delivery of anticancer drugs. We achieved this by co-loading the FDA-approved NIR-adsorbing dye, ICG, with a model drug, Dox, into PLGA NPs. Following intravenous administration, the developed drug-loaded NPs

[a] Department of Pharmaceutical Sciences, North South University, Dhaka-1229, Bangladesh. E-mail: shazid.sharker@northsouth.edu

[b] Department of Pharmaceutical Technology, University of Dhaka, Dhaka-1000, Bangladesh

[c] Department of Physics and Chemistry, Daegu Gyeongbuk Institute of Science and Technology (DGIST), Daegu, Republic of Korea

† Electronic supplementary information (ESI) available. See DOI: https://doi.org/10.1039/d3ma00375b

‡ These authors have contributed equally to this work.

Scheme 1 (a) The chemical composition of the developed NPs: both doxorubicin (Dox) and indocyanine green (ICG) were co-loaded into poly(lactic-*co*-glycolic acid) (PLGA). (b) Working principle of the developed NPs upon NIR irradiation. The biodegradable nanoscale PLGA NPs can be tumor-targeted (passive) by using an improper drainage system/acidic pH/porous leaky vasculature and generate area-specific photothermal heat in response to NIR light exposure.

(Dox–ICG-loaded PLGA) generate heat locally through photothermal conversion upon NIR light irradiation (Scheme 1). This NP-mediated temperature change can be monitored in real time to track the localization of NPs within the tumor. To assess their effectiveness in cancer therapy, we conducted *in vivo* experiments with DMBA/TPA-induced tumor-bearing mice to confirm the feasibility of these synthesized NPs.

2. Materials and methods

2.1. Materials

Poly(lactic-*co*-glycolic acid) (PLGA) with lactide : glycolide (50 : 50) with a molecular weight of 30 000–60 000, polyvinyl alcohol (PVA) with an 88% hydrolyzation degree, DMBA, TPA and indocyanine green (ICG) were purchased from Sigma-Aldrich, Germany. Doxorubicin (Dox) was obtained as a gift from Beacon Pharmaceuticals Ltd, Dhaka, Bangladesh. The remaining reagents and solvents utilized in this study were analytical grade.

2.2. PLGA NP synthesis and drug loading

Poly(D,L-lactide-*co*-glycolide) (PLGA) nanoparticles (NPs) were prepared using an emulsification solvent diffusion method with polyvinyl alcohol (PVA) as the stabilizer.[12] First, PLGA, the anticancer drug (doxorubicin), and ICG were dissolved in dichloromethane (DCM). Then this solution was added dropwise to the surfactant (PVA) under mild to vigorous magnetic stirring. The pre-emulsion was then homogenized (12 000 rpm, 5 min) using a high-speed homogenizer (HQ-2475, MXBAO-HENG, China). The water phase promotes the diffusion of the organic phase into the external phase, leading to the formation of PLGA nanoparticles (NPs). Lastly, the organic phase was

evaporated with continuous magnetic stirring for 10–12 h. The prepared NPs were then freeze-dried for further studies.

2.3. Characterizations

A Xintest HT-02 NIR thermal imaging camera and an 808 nm, 2 W cm^{-2} portable NIR laser (China) were used. Ultraviolet and visible (UV-vis) spectral absorptions were recorded using a UV-1800 Shimadzu spectrophotometer (Kyoto, Japan). Fourier-transform infrared (FT-IR) measurements were conducted in the ATR (attenuated total reflection) mode in the region from 400 to 4000 cm^{-1} by using infrared (IR) spectroscopy (iR Affinity 1, Shimadzu, Japan). The (%) transmission spectra were measured at 2 cm^{-1} resolution. ^{1}H NMR spectroscopy was conducted using a Bruker AVANCE 400 NMR spectrometer with d$_6$-DMSO as the solvent.

The chemical compositions of NPs were assayed by ATR-IR and energy-dispersive X-ray (EDX) spectroscopy. Scanning electron microscopy (SEM) was used to determine the size, shape, and structural properties. The polydispersity index (PDI), zeta potential, and behaviour in liquid media were studied using dynamic light scattering (DLS) and zeta potential measurements (Malvern Zetasizer).

The size (diameter, nm), polydispersity index, and surface charge (zeta potential, mV) of the PLGA NPs and drug/dye-loaded PLGA NPs were determined using a Zetasizer (Malvern Instruments Ltd, Malvern, UK) equipped with a He–Ne laser with a wavelength of 633 nm and a fixed scattering angle of 90°. Determinations were performed at 25 °C for samples appropriately diluted in Milli-Q water.

2.4. Scanning electron microscopy (SEM) imaging and energy-dispersive X-ray (EDX) spectroscopy

The particle size and surface features of PLGA NPs and drug/dye-loaded PLGA NPs were studied using field emission scanning electron microscopy (FE-SEM; model: JSM-6700, JEOL Ltd, Japan). The NP samples were prepared by spreading them on an aluminium foil. The blank, ICG-loaded PLGA NPs, Dox-loaded PLGA NPs and Dox–ICG-loaded PLGA NPs were sputter-coated with a gold–palladium alloy for boosting the electrical conductivity to obtain high-resolution SEM images and energy-dispersive X-ray (EDX) spectra for composition analysis. Finally, all SEM images were taken using an acceleration voltage of 5 kV or 15 kV.

2.5. *In vitro* release kinetics of drug-loaded NPs

The loading content and loading efficiency were determined by using UV-visible spectroscopy (λ_{max} = 480 nm), where the number of samples exceeded five. The loading content can be calculated as [drug-loaded PLGA NP weight – bare PLGA NP weight] × 100/(drug-loaded PLGA NP weight). The loading efficiency can be calculated as [Dox (total) − Dox (no deposited) × 100/Dox (total)].[13] The Dox loading content and loading efficiency on Dox–ICG-loaded PLGA NPs were 1% (w/w) and 86%, respectively.

The release behaviour of drugs from Dox–ICG-loaded PLGA NPs was evaluated at 36 °C and different pH values of 4.0, 5.5,

and 7.4 with or without 5 min NIR irradiation in PBS buffer medium (10 mmol) inside dialysis chambers (with a molecular weight cut-off equal to 3500) against water.[6] To determine the amount of drug released, a 3 mL solution was taken from the outside released medium, and 3 mL of the solution was replaced by the new-release medium. The absorbances were measured at 480 nm using UV-visible spectroscopy; the amount (%) of the drug released was then calculated.

2.6. *In vivo* studies

The animals were housed under standard laboratory conditions (relative humidity: 55–65%, room temperature: 23 ± 2 °C, and 12 h light/dark cycle). Adult Swiss albino mice of either sex aged 7–8 weeks and weighing 30–35 g were obtained from the animal house of the Department of Pharmaceutical Sciences, North South University (NSU). The animals were fed with a standard diet and water *ad libitum*. The NSU Institutional Animal Care and Use Committee (IACUC) approved (IACUC ID: 2021/OR-NSU/IACUC/1103) the experimental protocol (SRC ID: CTRG-21-SHLS-01).

2.7. *In vivo* tumor (skin carcinogenesis) model

The *in vivo* tumor was induced in mice according to the method reported in the literature.[14] For instance, under ketamine anaesthesia, the mice were shaved on the back skin for topical application of 7,12-dimethylbenzanthracene (DMBA) and 12-O-tetradecanoylphorbol-13-acetate (TPA). DMBA (50 µg/200 µL) was applied topically once on the shaved area using a pipette. TPA (5 µg/200 µL) was then applied after one week, topically with a micropipette twice a week. A palpable mass greater than 1 mm in diameter was considered a papilloma and tumor. The recorded tumor volume (mm[3]) can be calculated as π/6 × (length × width × height).[15] The mice bearing skin tumours were treated with a chemotherapeutic drug in the presence or absence of mild photothermal heat treatment.

2.8. *In vivo* treatments

When the tumor grew 15 ± 2 mm[3] in volume, 200 µL of sterile water for injection (SWFI) containing Dox (free), Dox-loaded PLGA NPs or Dox–ICG-loaded PLGA NPs at 30 mg per kg per one-dose per week (body weight) was injected for five weeks into the mice tail vein (*n* = 5 per group). After a one-hour post-injection period every week, the tumours were irradiated using a NIR laser (photothermal heat) and maintained at 45 °C for 5 min.[16–18] In the following steps, the therapeutic results of each group were evaluated by measuring the tumor volumes for five weeks. The survival of all animals was recorded over that period. For histological analysis, tumor tissues were excised from the mice in the sixth week. The sliced tumor tissues (6 µm) were stained with haematoxylin and eosin (H&E) and observed with an optical microscope.[18] The combination index (CI) of Dox–ICG-loaded PLGA NPs for synergistic cancer therapy was calculated in the absence and presence of photothermal heat. The derived combination index equation (CIE) for two types of treatment is as follows: CI = D1/Dx1 + D2/Dx2.[19] Here, Dx1 and Dx2 are the two doses (min and max concentrations)

used to recover in the absence of photothermal heat, and D1 and D2 are the two doses (concentrations) used to recover from the tumour in the presence of photothermal heat. The complete design of the *in vivo* experimental mice model was followed accordingly.

3. Results and discussion

The goal of this study was to develop a nanoparticle (NP) based drug delivery system (DDS) for doxorubicin (Dox) and improve the antitumor activity by photothermal stimuli. PLGA was selected for the preparation of NPs for its biodegradability and biocompatibility.[8] In this study, Dox and the NIR responsive indocyanine green (ICG) dye were loaded into PLGA NPs. Fig. S1 (ESI†) shows the photo images of the purified PLGA NPs (blank), ICG dye-loaded PLGA NPs, Dox-loaded PLGA NPs, and drug-ICG-loaded PLGA NPs during synthesis. The UV-visible spectra show PVA and PLGA, the precursor of PLGA NPs (Fig. 1a). The PVA optical absorption shows a sharp peak near 223 and two broad peaks near 282 and 327 nm.[20] The free PLGA shows a strong peak near 210 nm and a narrow peak near 300 nm.[21] The NPs were prepared using PLGA as the precursor polymer and PVA as the surfactant. As a result, the PLGA NPs showed a broad spectrum from 200 to 400 nm without a defined peak. At the same time, the ICG-loaded PLGA NPs showed a defined spectrum near 800–810 nm as an indication of this NIR (ICG) dye.[22] Additionally, the Dox–ICG-loaded PLGA NPs retain the previous broad spectrum with an additional peak near 480–500 nm, demonstrating the simultaneous loading of doxorubicin.[13] At the same time, the UV-visible absorption spectrum exhibited an increased baseline level for all PLGA NPs. This might be due to the particle nature and optical absorbance properties of all PLGA-based NPs.

The FT-IR spectra of PLGA NPs, ICG-loaded, Dox-loaded, and ICG–Dox-loaded PLGA NPs showed characteristic peaks in their selected area (Fig. 1b). The PLGA NP bands of the spectrum near 1760 cm^{-1} correspond to the carbonyl (–C=O) of the

Fig. 1 Characterization of the chemical formulations of PLGA NPs. (a) UV-visible absorption spectra of PVA, PLGA, PLGA NPs, ICG-loaded PLGA NPs, Dox-loaded PLGA NPs and Dox–ICG-loaded PLGA NPs. (b) The FT-IR transmission peaks of blank PLGA NPs, ICG-loaded PLGA NPs, Dox-loaded PLGA NPs and Dox–ICG-loaded PLGA NPs.

lactone, the 1459 cm^{-1} peak to the C–H bending of the CH$_3$ group, and the 1423 cm^{-1} peak to the CH bending of the O–CH group of glycolic acid.[23] The PLGA NPs were used to load ICG for NIR responsiveness and photothermal conversion efficiency. The ICG dye-loaded PLGA NPs exhibited a C=C (aromatic) stretching peak at 1400–1500 cm^{-1}, and (C–H) vinyl stretching occurred at 900–1100 cm^{-1} and a C–H out-of-plane bending peak was observed at 600–1000 cm^{-1}.[5,24] To investigate the antitumor activity, doxorubicin (Dox) was also loaded into the PLGA NP system. The Dox-loaded PLGA NPs showed characteristic IR peaks near 2933 cm^{-1} for C–H and 1083 cm^{-1} for C–O groups with peaks near 805 and 688 cm^{-1} corresponding to C=H bending and the C=C bond in the ring.[25,26] The characteristic FTIR transmission peaks of ICG and Dox in ICG–Dox-loaded PLGA NPs can confirm the successful loading in PLGA NP carriers.

The PLGA NPs were characterized by ^{1}H-NMR spectroscopy analysis (Fig. 2). The peak near δ 1.55 ppm of PLGA NPs is attributed to the methyl protons of D- and L-lactic acid repeated monomer of PLGA. At the same time, the peak near δ 5.2 ppm is assigned to the CH proton of lactic acid and that near δ 4.8 ppm to the CH$_2$ group of glycolic acid.[23] The ^{1}H-NMR spectrum of ICG-loaded PLGA NPs indicated additional peaks around δ 4.23 ppm for the CH$_2$ protons of the alkyl chain and the CH proton of the benzene ring near δ 7.96–7.98, 7.60, and 7.45 ppm.[27] At the same time, the Dox-loaded PLGA NPs showed peaks around δ 1.18 (d, 3H, CH$_3$), δ 4.17 (m, 1H), δ 3.93 (S, 3H, OCH$_3$), δ 5.30 (S, 1H, H11), δ 4.93 (1H) and δ 7.90–7.92 (m, 2H, H3, H4).[28] These characteristic proton peaks for doxorubicin indicate its successful loading into PLGA nanoparticles. Combining Dox and ICG in the PLGA NP delivery system (Dox–ICG-loaded PLGA NPs) retains most of their precursor proton peaks, and some overlap and slightly shifted signals (Fig. 2d). Therefore, most of the proton peaks in Dox–ICG-loaded PLGA NPs demonstrated the presence of doxorubicin and ICG dye.

Scanning electron microscopy (SEM) image analysis was carried out for the PLGA NPs to examine their size, shape, and structural compositions (Fig. 3). The particles had a
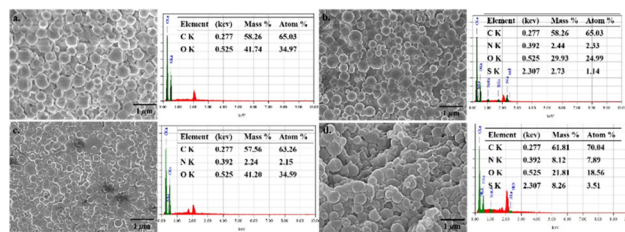

Fig. 3 Characterization of the morphology and size distribution of NPs. The scanning electron microscopy (SEM) images (scale bar: 1 μm) of (a) PLGA NPs, (b) ICG-loaded PLGA NPs, (c) Dox-loaded PLGA NPs and (d) Dox–ICG-loaded PLGA NPs. Representative energy dispersive X-ray (EDX) spectroscopy analysis for the elemental (C, carbon; N, nitrogen; O, oxygen; S, sulphur) compositions of the respective samples.

diameter of 100–180 nm with a spherical shape. The SEM images of PLGA NPs before and after loading with the ICG dye and Dox drug are shown in Fig. 3. The SEM images of the NPs revealed a smooth, uniform surface in the case of blank PLGA NPs, whereas ICG-, Dox-, and Dox–ICG-loaded particles showed slightly irregular surfaces. The loaded agents into PLGA NPs distributed asymmetrically and randomly during NP formation.[29] These can be attributed to the autonomous propelling of different PLGA, Dox, and ICG groups on the particle surface after completing the NP synthesis (Fig. S2, ESI†).

The EDX (SEM/EDX) spectra showed the elemental contents in PLGA NPs. In the EDX spectra, the indication of sulphur (S) element is owing to the presence of ICG in ICG-loaded PLGA NPs. The nitrogen (N) element originated due to the presence of doxorubicin in Dox-loaded PLGA NPs. At the same time, the presence of C and O elements as the base elements of these NP delivery systems was mainly due to the PLGA polymer.[29] The elemental distribution of Dox–ICG-loaded PLGA NPs showed an asymmetric distribution of N and S elements after the functionalization and loading process. The N element content on the PLGA NP surface increased from 2.15 to 7.89% in Dox-loaded and Dox–ICG-loaded PLGA NPs. EDX elemental analysis focused on ICG-loaded and Dox–ICG-loaded PLGA NPs, revealing the presence of 1.14% and 3.51% S, respectively. However, blank PLGA NPs showed no trace S element. The embedded ICG in PLGA NPs was the reason for the presence of a trace amount of the S element.[30]

The XRD patterns of blank PLGA NPs, ICG-loaded PLGA NPs, Dox-loaded PLGA NPs, and Dox–ICG-loaded PLGA NPs are shown in Fig. S3a (ESI†). The XRD 2θ peaks of Dox showed sharp scattering angles near 15–25° and 8–16°, respectively. On the other hand, the diffraction pattern of free ICG exhibited a non-specific broad XRD pattern.[31] At the same time, no characteristic peaks appeared in Dox-loaded PLGA NPs, similar to blank PLGA NPs. The XRD scattering angles of the blank and drug-loaded PLGA NPs exhibited broader and weaker peaks. The absence of sharp XRD 2θ peaks can be related to a semi-crystalline structure due to an extensive PLGA-based NP system. This indicates loading and encapsulation of Dox and ICG in Dox–ICG-loaded PLGA NPs.[32] The result proves that PLGA NPs can retain their original amorphous structure after loading of both ICG and Dox.

Fig. 2 Characterization of the chemical structures of the synthesized NPs. ^{1}H-NMR (d$_6$-DMSO) spectra of (a) blank PLGA NPs and (b) ICG-loaded PLGA NPs with magnified area (3.2 to 4 δ and 0.8 to 2.7 δ) (green colour), (c) Dox-loaded PLGA NPs (red colour), and (d) Dox–ICG-loaded PLGA NPs with magnified area (0.8 to 2.7 δ and 3.2 to 5.4 δ), respectively.

The surface charge of the prepared NPs was measured by zeta potential (mV) distribution. The blank PLGA NPs showed an average negative zeta potential of −50 mV (Fig. S3b, ESI†). Native PLGA NPs contained anionic acidic functional groups, indicating negative surface charges. At the same time, ICG-loaded PLGA NPs, Dox-loaded PLGA NPs, and Dox–ICG-loaded PLGA NPs exhibited average zeta potentials of −31 mV, −13 mV, and +16 mV, respectively. The charge of blank PLGA NPs slightly decreased with the loading of ICG, which indicated shielding of the negative surface charges. Indeed, Dox-loaded PLGA NPs showed a decreased negative potential as the Dox contained positively charged groups. The Dox–ICG-loaded PLGA NPs retained positive potential owing to the neutralization of native surface charges and positive functional group residues.[31] The positive +mV zeta potential is effective for cell surface anchoring, absorption, and delivery of therapeutic payload.

The hydrodynamic volumes of blank PLGA NPs, ICG-loaded PLGA NPs, Dox-loaded PLGA NPs, and Dox–ICG-loaded PLGA NPs were measured by DLS (dynamic light scattering) (Fig. S4, ESI†). The average diameter of blank PLGA NPs was 120 nm (polydispersity index, PDI = 0.99), that of ICG-loaded PLGA NPs was 130 nm (PDI = 0.65), that of Dox-loaded PLGA NPs was 180 nm (PDI = 1), and that of Dox–ICG-loaded PLGA NPs was 140 nm (PDI = 0.75). This can explain that solvent evaporation and polymer diffusion determine particle size-related properties. The chemical nature of the loaded small molecular ICG and Dox in the PLGA NP system is believed to contribute to the solvent evaporation rate and diffusion rate, which could be a reason for the different sizes, size distributions, and different PDIs.[12]

The loaded ICG photosensitizes the PLGA NPs, which can generate heat from light absorption at a specific location. The photothermal heat generation capability of PLGA NPs, Dox-loaded PLGA NPs, ICG-loaded PLGA NPs, and Dox–ICG-loaded PLGA NPs was studied in response to NIR irradiation (808 nm).[5] The results showed that the temperature substantially increased (∼42 °C in 5 minutes) in the case of ICG-loaded PLGA NPs and ICG–Dox-loaded PLGA NPs (Fig. 4). In contrast, Dox-loaded PLGA NPs showed a lower level of photothermal conversion. At the same

time, the photothermal efficiency of Dox–ICG-loaded PLGA NPs showed that increasing temperature is time and concentration-dependent. In the presence of NIR light, the temperature increased from 26 to 42 °C when the concentration was 1 to 0.001 mg mL^{-1}. Such heat is very effective for *in vivo* applications in photothermal therapy (PTT) and temperature-responsive drug delivery systems (DDS).[33] Additionally, the photothermal conversion efficiency (η) of Dox–ICG-loaded PLGA NPs was calculated based on the energy balance of the system (Fig. S5, ESI†).[4] The η value of Dox–ICG-loaded PLGA NPs in water was 30.80% which is comparable to those of other ICG encapsulated polymeric nanoparticles.[34]

The *in vitro* cumulative drug release from Dox–ICG-loaded PLGA NPs was studied at different pH values (4.0, 5.5, and 7.4) without and with photothermal heat.[6] Fig. 5a and b shows that the cumulative release of Dox was increased in acidic pH and the presence of NIR irradiation. At 36 °C (body temperature), the cumulative release of Dox was 45%, 49%, and 55% after six hours when the pH was 7.4, 5.5, and 4.0, respectively. In contrast, the Dox release rate was 50%, 55%, and 62% under NIR light irradiation. Such temperature can be generated at the tumor site after PLGA NP-loaded drug administration and NIR light treatment. Treating the PLGA NPs at a higher temperature induced favourable dissolution and enhanced the release rate. At the same time, the rate of release can be increased in acidic environments like those with pH 4–5.5. At the same time, the study of ICG release from Dox–ICG-loaded PLGA NPs under the same experimental conditions showed almost similar kinetics to those observed above (Fig. S6, ESI†). This is because acidic pH helps protonation/ionization to accelerate Dox from PLGA NP carriers.[35–37] The effective Dox release was reported at higher temperatures and lower pH values.[38,39] It can be synergistically enhance the efficacy of chemotherapy, PTT, immunotherapy, and other cancer therapies.[40–42]

The acidic pH response can be successfully utilized in the PLGA NP system as the cellular organelles and tumor microenvironments are typically acidic. The photothermal heat at 5 h, 10 h, and 15 h time points showed moderately increased drug release from PLGA NP carriers (Fig. S7, ESI†). However, the impact of NIR heat was slightly decreased on drug release at 10 h and 15 h of observation compared to 5 min and 5 h points.

Fig. 4 Comparison of the photothermal conversion efficiency of the synthesized NPs in different formulations. (a) The temperature elevation curves of blank PLGA NPs, Dox-loaded PLGA NPs, ICG-loaded PLGA NPs, and Dox–ICG-loaded PLGA NPs in response to 5 min NIR irradiation (808 nm laser, 2 W cm^{-2}). (b) The concentration-dependent thermal heat generated curve of Dox–ICG-loaded PLGA NPs as a function of NIR irradiation time.

Fig. 5 Drug release profiles of the synthesized NPs upon pH variation. (a) The pH-responsive *in vitro* (%) drug release of Dox–ICG-loaded PLGA NPs. The release medium pH was 7.4, 5.5, and 4.0 and the temperature was 36 °C. (b) The heat-responsive *in vitro* drug release in response to 5 min NIR irradiation (808 nm laser, 2 W cm^{-2}). The NIR light was used at the beginning of the drug release study.
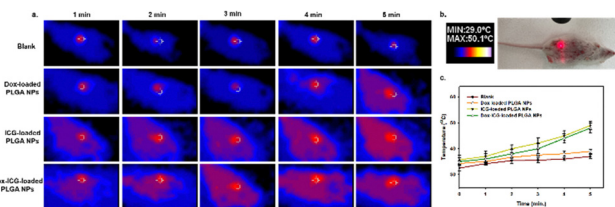
1

Fig. 6 Evaluation of *in vivo* photothermal conversion upon NIR light irradiation. (a) The *in vivo* thermograph in response to NIR laser treatment on mice tumor. The images were recorded after tail vein administration of blank PLGA NPs (control group), Dox-loaded PLGA NPs, ICG-loaded PLGA NPs, and Dox–ICG-loaded PLGA NPs. (b) A representative photo-image of tumor-bearing mice with NIR laser irradiation and (c) *in vivo* photothermal heat generation curve in response to different NIR irradiation times (mean $\pm$ SD, $n = 5$). The NIR laser irradiation and temperature were recorded one hour post-injection at first therapy. An 808 nm, 2 W cm^{-2} laser was used.

Fig. 7 Evaluation of the *in vivo* anticancer efficiency of the developed NPs. (a) The photo images (before and after treatment) of tumor bearing mice treated with no drug (control group), free drug (Dox), Dox-loaded PLGA NPs, Dox–ICG-loaded PLGA NPs and Dox–ICG-loaded PLGA NPs under 5 min NIR laser irradiation. (b) The *in vivo* anticancer activity was measured by observing the tumor volume (mm^3) size reduction in the blank group (control group) and mice treated with free Dox, Dox-loaded PLGA NPs, Dox–ICG-loaded PLGA NPs and Dox–ICG-loaded PLGA NPs under 5 min NIR laser irradiation. (c) The *Kaplan–Meier* curve for the (%) survival was recorded during the anticancer activity of mice (mean $\pm$ SD, $n = 5$). (d) The photo images of the tumor were collected from the sacrificed mice treated with (I) Dox–ICG-loaded PLGA NPs under 5 min NIR laser light irradiation, (II) Dox–ICG-loaded PLGA NPs, (III) Dox-loaded PLGA NPs, (IV) free drug (Dox) and (I) no drug (control group). The NIR laser irradiation was performed one hour post injection. An 808 nm, 2 W cm^{-2} laser was used. (Error bars were based on standard deviations ($\pm$SD) and $n = 5$ per group where ***$p < 0.001$ was determined by Student's *t* test value.)

In tumor-bearing mice, the photothermal conversion efficiency was studied after administering Dox-loaded PLGA NPs, ICG-loaded PLGA NPs, and Dox–ICG-loaded PLGA NPs upon NIR laser irradiation (Fig. 6). The *in vivo* thermographs were recorded using a NIR thermal camera, and each tumor surface was irradiated for up to five minutes one hour post injection (tail vein).[19] The figure shows no noticeable temperature generation in the control group (blank). The Dox-loaded PLGA NPs showed almost the same result as the control group, *i.e.* no noticeable temperature changes on the tumor surface. At the same time, ICG-loaded PLGA NPs and Dox–ICG-loaded PLGA NPs exhibited increased surface temperature in response to NIR irradiation. Indocyanine green (ICG) dye with strong NIR absorbance has been proven as an effective photothermal agent. In the presence of NIR light, the ICG-based NPs generate vibrational energy to translate into heat energy owing to photothermal conversion. The tumor surface temperature measured with the IR thermal camera raised from 36° to 48 °C steadily within five minutes, in contrast to control and Dox-loaded PLGA NPs. The similar NIR-responsive photothermal heat was overserved up to the fifth therapy (five weeks) in every tumor-bearing mouse group. The laser-treated photothermal heat can be increased in the necrotic area in tumours through irreversible damage to the cellular structure. Such photothermal ablation, known as photothermal therapy (PTT), can kill cancer cells when the temperature is maintained at 42 °C for 15–60 minutes.[4,43–45] Additionally, it is suggested that chemotherapy drugs combined with PTT can synergistically work to eradicate malignant tumours biologically and thermally.[19]

For the evaluation of *in vivo* antitumor therapeutic activity, the free drug (Dox) and Dox-loaded PLGA NPs were investigated against the DMBA-initiated and TPA-promoted mice tumor models on the skin (Fig. 7). The representative photo images showed that DMBA/TPA treatment induced tumors in mice.[14] The tumor-bearing mice were injected in the tail vein with a free drug (Dox), Dox-loaded PLGA NPs, and Dox–ICG-loaded PLGA NPs without and with 5 min NIR laser irradiation.[6] The six week observation showed a decreased tumor size compared with the control group. A difference in size reduction was observed in Dox–ICG-loaded PLGA NP-treated mice, which

was remarkably reduced when NIR irradiation was applied in the treatment group.

The tumor (15 $\pm$ 2 mm^3) grows noticeably after eight weeks of DMBA/TPA application on the skin of mice. In the control group, a number of mice showed burst carcinogen exposure, and the tumor size and number continuously increased compared to free Dox-loaded and different Dox-loaded PLGA NP groups (Fig. S8, ESI†). All mice were treated once weekly at 30 mg kg^{-1} body-weight dose for five weeks. The tumor grew heterogeneously and showed variations in different mice before treatments. However, injection of Dox-loaded PLGA NPs and Dox–ICG-loaded PLGA NPs in the tail vein noticeably suppressed tumor development in terms of the area and average number. The mice treated with Dox–ICG-loaded PLGA NPs with five minutes of NIR-based photothermal irradiation of the tumor area showed the disappearance of the visible tumor. This might be because the generated photothermal heat on the tumor area facilitated improved drug deposition, followed by synergistic ablation of the tumor.[46,47] The combination index (CI) values showed values < 1, which quantitively suggested a synergistic effect in the presence of photothermal heat on the tumours of mice.[19]

The average body weights of mice treated with Dox, Dox-loaded PLGA NPs, Dox–ICG-loaded PLGA NPs, and Dox–ICG-loaded PLGA

NPs under NIR light irradiation were recorded (up to 6 weeks) to monitor their health condition (Fig. S9, ESI†). In the initial stages, all mice showed slightly increased body weight. A few weeks later, the body weight in the PLGA NP treatment group remained unchanged. However, the control group mice showed different body weights up to the 6th week, where the last therapy was given in the 5th week. At the same time, the mice treated with free Dox showed decreased average body weight after the treatment started. This shows that chemotherapy related side-effects hamper regular physiological activity and weak health conditions.[48]

It should be noted that the PLGA NPs loaded with Dox maximized the anticancer efficacy of ICG-mediated photothermal heat. The results could be attributed to the following two reasons: first, the Dox–ICG-loaded PLGA NPs were efficiently internalized by the acidic tumor microenvironment and leaky blood vessels, thus significantly facilitating intracellular Dox delivery. Second, the internalized Dox–ICG-loaded PLGA NPs with mild photothermal heat could aid the trafficking of Dox from PLGA NPs close to nuclei to boost its anticancer potency. Based on these findings, it can be concluded that the Dox–ICG-loaded PLGA NPs with NIR-triggered heat in this work can be a promising approach for efficient cancer therapy.[49]

The survival analysis during the *in vivo* study showed that 60% of mice died after the first week in the control group (Fig. 7c). At the same time, the other group maintained a 90% survival rate. The survival percentages slightly decreased by 75% in the free Dox-treated group, whereas the PLGA-based NP group maintained a 90% survival rate. Thus, the results suggest the overall therapeutic benefits of chemotherapeutic-loaded PLGA NP systems.[4] At the end of the *in vivo* study, the tumor tissues were collected from the sacrificed mice in the 6th week (after five week therapy) (Fig. 7d). The image results and scale bars also suggested that Dox–ICG-loaded PLGA NPs with photothermal heat can significantly reduce the incident and tumor area.[50]

In the histological analysis, the control group and different treatment groups were studied to compare the effects of an anticancer drug (Dox) with photothermal heat on tumor size reduction (Fig. 8). The tissues were collected after six weeks

from the tumor area of sacrificed mice. The haematoxylin and eosin (H&E) staining optical images were used in this evaluation. The control (no treatment) group tumor section showed a thick (mm scale) epithelial layer with hyperkeratosis and keratin pearl, an indicator of squamous cell carcinoma.[15] At the same time, the tumour sections of the treatment groups exhibited a decreased epithelial layer. Such changes can be explained by control differentiation and cell growth.[51] The epithelial layer was significantly reduced (μm range) in the Dox–ICG-loaded PLGA NP treatment group, and it appeared like a healthy skin layer when Dox–ICG-loaded PLGA NPs with 5 min NIR laser irradiation were applied. This result indicated that photothermal heat with Dox–ICG-loaded-PLGA NPs substantially inhibited tumor growth.[52,53]

4. Conclusions

Chemotherapeutic drugs have long been used as a cost-effective and primary choice of medication for cancer treatment. Consequently, there is a strong desire to achieve area-specific cytotoxic effects and maximize drug accumulation at the tumor site *in vivo*. This study focused on achieving area-selective action through the systemic administration of Dox–ICG-loaded PLGA NPs, facilitated by localized heat generated by photothermal conversion. The nanoscale particle size and elemental compositions were characterized using SEM/EDX, DLS, XRD, FT-IR, and 1H-NMR spectroscopy. The NIR response and photothermal heat generation were found to be time- and concentration-dependent. The convenience of using NIR light as a heat-generating tool in conjunction with Dox–ICG-loaded PLGA NPs holds promise for advancing various chemotherapy combinations. We have observed significant improvements in tumor size, number, and histology following this approach. A NIR-guided PLGA NP formulation of Dox has wide applicability in synergistic anticancer therapies for solid tumours.

Author contributions

Tunazzina Zaman Khan and Shekh Md Newaj: writing – original draft, visualization. Ashikur Rahman: validation, methodology, investigation. Rahnuma Tabassum and Khandaker Nujhat Tasnim: formal analysis, data curation. Shazid Md. Sharker: supervision, resources, project administration, methodology, investigation. Md. Selim Reza, Hasan Mahmud Reza, Seonki Hong and Shazid Md. Sharker: writing – review & editing.

Conflicts of interest

There are no conflicts to declare.

Acknowledgements

Fig. 8 Evaluation of tumor growth suppression by NIR-derived photo-chemotherapy. The Hematoxylin and eosin (H&E) staining images of the tumor tissue sections of mice treated with (a) no drug (control group), (b) free Dox (drug), (c) Dox-loaded PLGA NPs, (d) Dox–ICG-loaded PLGA NPs and (e) Dox–ICG-loaded PLGA NPs under 5 min NIR laser irradiation. The scale bar is 25 μm, and images are recorded at 10× magnification. The (vertical) line bar indicates the thickness of the epithelial cell.

References

1 D. Peer, J. M. Karp, S. Hong, O. C. Farokhzad, R. Margalit and R. Langer, 84 Nat nanotech 2007 R Langer Nanocarriers as an emerging platform for cancer therapy, *Nat. Nanotechnol.*, 2007, **2**, 751–760.

2 E. S. Ali, S. M. Sharker and M. T. Islam, *et al.*, Targeting cancer cells with nanotherapeutics and nanodiagnostics: Current status and future perspectives, *Semin. Cancer Biol.*, 2021, **69**, 52–68.

3 M. Rahman, F. Chowdhury, K. Uddin, K. S. Ahmed, H. Hossain, P. Jain, H. M. Reza, K. Lee and S. M. Sharker, Nanostructured chitosan-polyphenolic patch for remote NIR-photothermal controlled dermal drug delivery, *Int. J. Biol. Macromol.*, 2023, **241**, 124701.

4 S. M. Sharker, S. M. Kim and J. E. Lee, *et al.*, Functionalized biocompatible WO3 nanoparticles for triggered and targeted in vitro and in vivo photothermal therapy, *J. Controlled Release*, 2015, **217**, 211–220.

5 S. M. Sharker, J. E. Lee and S. H. Kim, *et al.*, pH triggered in vivo photothermal therapy and fluorescence nanoplatform of cancer based on responsive polymer-indocyanine green integrated reduced graphene oxide, *Biomaterials*, 2015, **61**, 229–238.

6 S. M. Sharker, S. M. Kim, S. H. Kim, I. In, H. Lee and S. Y. Park, Target delivery of β-cyclodextrin/paclitaxel complexed fluorescent carbon nanoparticles: Externally NIR light and internally pH sensitive-mediated release of paclitaxel with bio-imaging, *J. Mater. Chem. B*, 2015, **3**(28), 5833–5841.

7 D. Peer, J. M. Karp, S. Hong, O. C. Farokhzad, R. Margalit and R. Langer, Nanocarriers as an emerging platform for cancer therapy, *Nano-Enabled Med. Appl.*, 2020, 61–91.

8 G. Cappellano, C. Comi, A. Chiocchetti and U. Dianzani, Exploiting PLGA-based biocompatible nanoparticles for next-generation tolerogenic vaccines against autoimmune disease, *Int. J. Mol. Sci.*, 2019, **20**(1), 204.

9 W. Zhen, W. Hu, L. Dong, S. An and X. Jiang, Nanomaterials for the regulation of the tumor microenvironment and theranostics, *Nanoscale Adv.*, 2020, **2**(4), 1395–1409.

10 S. M. Sharker, Nanoparticle for Photoresponsive Minimal-Invasive Cancer Therapy, *Cancer Nanotheranostics*, Springer, 2021, vol. 8, pp. 201–216.

11 S. M. Sharker, M. A. Alam, M. C. Shill, G. M. S. Rahman and H. M. Reza, Functionalized hBN as targeted photothermal chemotherapy for complete eradication of cancer cells, *Int. J. Pharm.*, 2017, **534**, 1–2.

12 S. Haque, B. J. Boyd, M. P. McIntosh, C. W. Pouton, L. M. Kaminskas and M. Whittaker, Suggested procedures for the reproducible synthesis of poly (d, l-lactide-*co*-glycolide) nanoparticles using the emulsification solvent diffusion platform, *Curr. Nanosci.*, 2018, **14**(5), 448–453.

13 E. B. Kang, S. M. Sharker, I. In and S. Y. Park, Pluronic mimicking fluorescent carbon nanoparticles conjugated with doxorubicin via acid-cleavable linkage for tumor-targeted drug delivery and bioimaging, *J. Ind. Eng. Chem.*, 2016, **43**, 150–157.

14 M. Vähätupa, T. Pemmari, I. Junttila, M. Pesu and T. A. H. Järvinen, Chemical-induced skin carcinogenesis model using dimethylbenz [a] anthracene and 12-o-tetradecanoyl phorbol-13-acetate (dmba-tpa), *J. Visualized Exp.*, 2019, **154**, e60445.

15 M. R. M. Roduan, R. Abd Hamid, H. Sulaiman and N. Mohtarrudin, Annona muricata leaves extracts prevent DMBA/TPA-induced skin tumorigenesis via modulating antioxidants enzymes system in ICR mice, *Biomed. Pharmacother.*, 2017, **94**, 481–488.

16 W. N. Keith, P. Joseph Mee and R. Brown, Response of mouse skin tumors to doxorubicin is dependent on carcinogen exposure, *Cancer Res.*, 1990, **50**(21), 6841–6847.

17 A. M. Gamal-Eldeen, S. M. El-Daly, I. H. Borai, H. A. Wafay and A. R. B. Abdel-Ghaffar, Photodynamic therapeutic effect of indocyanine green entrapped in polymeric nanoparticles and their anti-EGFR-conjugate in skin cancer in CD1 mice, *Photodiagn. Photodyn. Ther.*, 2013, **10**(4), 446–459.

18 S. H. Kim, J. E. Lee, S. M. Sharker, J. H. Jeong, I. In and S. Y. Park, In Vitro and in Vivo Tumor Targeted Photothermal Cancer Therapy Using Functionalized Graphene Nanoparticles, *Biomacromolecules*, 2015, **16**(11), 3519–3529.

19 T. C. Chou, The combination index (CI < 1) as the definition of synergism and of synergy claims, *Synergy*, 2018, **7**, 49–50.

20 E. Rusu, A. Airinei, V. Barboiu and D. Timpu, Some characteristics of poly (vinyl alcohol) with azido aromatic groups, *J. Optoelectron. Adv. Mater.*, 2007, **9**(4), 1044.

21 M. I. Torres-Ramos, M. F. Martín-Marquez, M. Leal-Moya, C. del, S. Ghotekar, J. A. Sánchez-Burgos and A. Pérez-Larios, PLGA–TiO2 as a Carrier System for Drug Release, *Int. J. Mol. Sci.*, 2022, **23**(18), 10755.

22 X. Zhang, N. Li and Y. Liu, *et al.*, On-demand drug release of ICG-liposomal wedelolactone combined photothermal therapy for tumor, *Nanomedicine*, 2016, **12**(7), 2019–2029.

23 H. Wang, Y. Zhao and Y. Wu, *et al.*, Enhanced anti-tumor efficacy by co-delivery of doxorubicin and paclitaxel with amphiphilic methoxy PEG-PLGA copolymer nanoparticles, *Biomaterials*, 2011, **32**(32), 8281–8290.

24 W. Li, H. Zhang and X. Guo, *et al.*, Gold nanospheres-stabilized indocyanine green as a synchronous photo-dynamic–photothermal therapy platform that inhibits tumor growth and metastasis, *ACS Appl. Mater. Interfaces*, 2017, **9**(4), 3354–3367.

25 R. Bansal, R. Singh and K. Kaur, Quantitative analysis of doxorubicin hydrochloride and arterolane maleate by mid IR spectroscopy using transmission and reflectance modes, *BMC Chem.*, 2021, **15**(1), 1–11.

26 L. E. Scheeren, D. R. Nogueira-Librelotto and L. B. Macedo, *et al.*, Transferrin-conjugated doxorubicin-loaded PLGA nanoparticles with pH-responsive behavior: a synergistic approach for cancer therapy, *J. Nanopart. Res.*, 2020, **22**, 1–18.

27 F. Rüttger, S. Mindt, C. Golz, M. Alcarazo and M. John, Isomerization and Dimerization of Indocyanine Green and a Related Heptamethine Dye, *Eur. J. Org. Chem.*, 2019, 4791–4796.

28 X. Li, C. Gao, Y. Wu, C. Y. Cheng, W. Xia and Z. Zhang, Combination delivery of Adjudin and Doxorubicin via integrating drug conjugation and nanocarrier approaches for the treatment of drug-resistant cancer cells, *J. Mater. Chem. B*, 2015, **3**(8), 1556–1564.

29 K. Bastari, M. Arshath and Z. H. M. Ng, *et al.*, A controlled release of antibiotics from calcium phosphate-coated poly (lactic-*co*-glycolic acid) particles and their in vitro efficacy against Staphylococcus aureus biofilm, *J. Mater. Sci.: Mater. Med.*, 2014, **25**, 747–757.

30 J. Wang, B. J. Toebes and A. S. Plachokova, *et al.*, Self-Propelled PLGA Micromotor with Chemotactic Response to Inflammation, *Adv Healthcare Mater.*, 2020, **9**(7), 1901710.

31 F. Xu, M. Liu and X. Li, *et al.*, Loading of indocyanine green within polydopamine-coated LAPONITE® nanodisks for targeted cancer photothermal and photodynamic therapy, *Nanomaterials*, 2018, **8**(5), 347.

32 F. Chai, L. Sun and X. He, *et al.*, Doxorubicin-Loaded Poly (Lactic-*co*-Glycolic Acid) Nanoparticles Coated with Chitosan/Alginate by Layer by Layer Technology for Antitumor Applications, *Int. J. Nanomed.*, 2021, **16**, 4187–4188.

33 S. Z. Akash, F. Y. Lucky and M. Hossain, *et al.*, Remote Temperature-Responsive Parafilm Dermal Patch for On-Demand Topical Drug Delivery, *Micromachines*, 2021, **12**(8), 975.

34 R. Ma, N. Alifu, Z. Du, S. Chen, Y. Heng, J. Wang, L. Zhu, C. Ma and X. Zhang, Indocyanine green-based theranostic nanoplatform for NIR fluorescence image-guided chemo/photothermal therapy of cervical cancer, *Int. J. Nanomed.*, 2021, **17**, 4847–4861.

35 T. Betancourt, B. Brown and L. Brannon-Peppas, Doxorubicin-loaded PLGA nanoparticles by nanoprecipitation: preparation, characterization and in vitro evaluation, *Future Med.*, 2007, 219–232.

36 F. Chowdhury, S. Ahmed, M. Rahman, M. A. Ahmed, M. D. Hossain, H. M. Reza, S. Y. Park and S. M. Sharker, Chronic wound-dressing chitosan-polyphenolic patch for pH responsive local antibacterial activity, *Mater. Today Commun.*, 2022, **31**, 103310.

37 M. L. Hakim, N. Nahar, M. Saha, M. S. Islam, H. M. Reza and S. M. Sharker, Local drug delivery from surgical thread for area-specific anesthesia, *Biomed. Phys. Eng. Exp.*, 2020, **6**(1), 015028.

38 R. A. Mustafa, M. Ran, Y. Wang, J. Yan, Y. Zhang, J. M. Rosenholm and H. Zhang, A pH/temperature responsive nanocomposite for chemo-photothermal synergistic cancer therapy, *Smart Mater. Med.*, 2023, **4**, 199–211.

39 T. Chen, W. Zeng, C. Tie, M. Yu, H. Hao, Y. Deng, Q. Li, H. Zheng, M. Wu and L. Mei, Engineered gold/black phosphorus nanoplatforms with remodeling tumor microenvironment for sonoactivated catalytic tumor theranostics, *Bioactive Mater.*, 2022, **10**, 515–525.

40 C. Lin, C. Huang, Z. Shi, M. Ou, S. Sun, M. Yu, T. Chen, Y. Yi, X. Ji, F. Lv and M. Wu, Biodegradable calcium sulfide-based nanomodulators for H2S-boosted Ca2 + -involved synergistic cascade cancer therapy, *Acta Pharm. Sin. B*, 2022, **12**, 4472–4485.

41 M. Ou, C. Lin, Y. Wang, Y. Lu, W. Wang, Z. Li, W. Zeng, X. Zeng, X. Ji and L. Mei, Heterojunction engineered bioactive chlorella for cascade promoted cancer therapy, *J. Controlled Release*, 2022, **345**, 755–769.

42 A. Yang, S. Sheng, Y. Bai, G. Xing, X. Yu, D. Zhu, L. Mei, X. Dong and F. Lv, Hydrogel/nanoparticles-mediated cooperative combination of antiangiogenesis and immunotherapy, *Acta Biomater.*, 2022, **153**, 124–138.

43 S. M. Sharker, Hexagonal boron nitrides (white graphene): A promising method for cancer drug delivery, *Int. J. Nanomed.*, 2019, 9983–9993.

44 S. H. Kim, S. M. Sharker, H. Lee, I. In, K. D. Lee and S. Y. Park, Photothermal conversion upon near-infrared irradiation of fluorescent carbon nanoparticles formed from carbonized polydopamine, *RSC Adv.*, 2016, **6**(66), 61482–61491.

45 T. R. Prianka, N. Subhan, H. M. Reza, M. K. Hosain, M. A. Rahman, H. Lee and S. M. Sharker, Recent exploration of bio-mimetic nanomaterial for potential biomedical applications, *Mater. Sci. Eng., C*, 2018, **93**, 1104–1115.

46 S. H. Adrita, K. N. Tasnim, J. H. Ryu and S. M. Sharker, Nanotheranostic Carbon Dots as an Emerging Platform for Cancer Therapy, *J. Nanotheranostics*, 2020, **1**(1), 59–78.

47 S. M. Sharker and M. Do, Nanoscale carbon-polymer dots for theranostics and biomedical exploration, *J. Nanotheranostics*, 2021, **2**(3), 118–130.

48 J. H. Doroshow, G. Y. Locker, I. Ifrim and C. E. Myers, Prevention of doxorubicin cardiac toxicity in the mouse by N-acetylcysteine, *J. Clin. Invest.*, 1981, **68**(4), 1053–1064.

49 C. W. Ting, Y. H. Chou, S. Y. Huang and W. H. Chiang, Indocyanine green-carrying polymeric nanoparticles with acid-triggered detachable PEG coating and drug release for boosting cancer photothermal therapy, *Colloids Surf., B*, 2021, **208**, 112048.

50 W. Wang, T. Jing, X. Xia, L. Tang, Z. Huang, F. Liu, Z. Wang, H. Ran, M. Li and J. Xia, *Biomater. Sci.*, 2019, **7**(10), 4060.

51 S. M. Sharker, S. M. Kim, J. E. Lee, J. H. Jeong, I. In, K. D. Lee, H. Lee and S. Y. Park, In situ synthesis of luminescent carbon nanoparticles toward target bioimaging, *Nanoscale*, 2015, **7**(12), 5468–5475.

52 S. M. Sharker, E. B. Kang, C. I. Shin, S. H. Kim, G. Lee and S. Y. Park, Near-infrared-active and pH-responsive fluorescent polymer-integrated hybrid graphene oxide nanoparticles for the detection and treatment of cancer, *J. Appl. Polym. Sci.*, 2016, **133**(32), 43791.

53 S. M. Sharker, Interaction of microwave and nanomaterials for thermoresponsive drug delivery and hyperthermal cancer therapy, *Inorg. Chem. Commun.*, 2023, 111152.